Mechatronics xxx (2013) xxx–xxx

Contents lists available at ScienceDirect

Mechatronics

journal homepage: www.elsevier.com/locate/mechatronics

Measuring and predicting resolution in nanopositioning systems

Andrew J. Fleming *

School of Electrical Engineering and Computer Science, The University of Newcastle, Callaghan 2308, NSW, Australia

ARTICLE INFO

Article history:
Received 23 May 2013
Revised 17 September 2013
Accepted 3 October 2013
Available online xxxx

Keywords:
Resolution
Noise
Nanopositioning
Motion control
Piezoelectric
Scanning probe microscopy

ABSTRACT

The resolution is a critical performance metric of precision mechatronic systems such as nanopositioners and atomic force microscopes. However, there is not presently a strict definition for the measurement or reporting of this parameter. This article defines resolution as the smallest distance between two non-overlapping position commands. Methods are presented for simulating and predicting resolution in both the time and frequency domains. In order to simplify resolution measurement, a new technique is proposed which allows the resolution to be estimated from a measurement of the closed-loop actuator voltage. Simulation and experimental results demonstrate the proposed techniques. The paper concludes by comparing the resolution benefits of new control schemes over standard output feedback techniques.

1. Introduction

A nanopositioning system is an electromechanical device for maneuvering an object in three or more degrees of freedom. A typical nanopositioner consists of base, a moving platform, actuators, position sensors, and a control system [1]. These devices are commonly used in scanning probe microscopes [2–5] to develop displacements of between one and one-hundred micrometers with a resolution on the order of one nanometer or less. Other applications of nanopositioning systems include nanofabrication [6–8], data storage [9], cell surgery [10], and precision optics [11].

Although the resolution is a key performance criteria in many applications, there is unfortunately no strict definition available in the literature. There are also no published industrial standards for the measurement or reporting of positioning resolution. Predictably, this has led to a wide variety of fragmented techniques used throughout both academia and industry. As a result, it is extremely difficult to compare the performance of different control strategies or commercial products.

The most reliable method for the measurement of resolution is to utilize an auxiliary sensor that is not involved in the feedback loop. However, this requires a sensor with less additive noise and greater bandwidth than the displacement to be measured. Due to these strict requirements, the direct measurement approach is often impractical or impossible. Instead, the closed-loop positioning noise is usually predicted from measurements of known noise sources such as the sensor noise.

In industrial and commercial applications, the methods used to measure and report closed-loop resolution vary widely. Unfortunately, many of these techniques do not provide complete information and may even be misleading. For example, the RMS noise and resolution is commonly reported without mention of the closed-loop or measurement bandwidth. In the academic literature, the practices for reporting noise and resolution also vary. The most common approach is to predict the closed-loop noise from measurements of the sensor noise [9,12]. However, this approach can underestimate the true noise since the influence of the high-voltage amplifier is neglected.

In this article, practical methods are described for the experimental characterization of resolution down to the atomic scale. Although the focus is on nanopositioning applications, the background theory and measurement techniques are applicable to any control system where resolution is a factor.

2. Resolution and noise

Since the noise sources that contribute to random position errors can have a potentially large dispersion, it is impractically conservative to specify a resolution where adjacent points never overlap. Instead, it is preferable to state the probability that the actual position is within a certain error bound. Consider the example

* Tel.: +61 2 4921 6493; fax: +61 2 4921 6993.
E-mail address: andrew.fleming@newcastle.edu.au

0957-4158/$ - see front matter © 2013 Elsevier Ltd. All rights reserved.
http://dx.doi.org/10.1016/j.mechatronics.2013.10.003

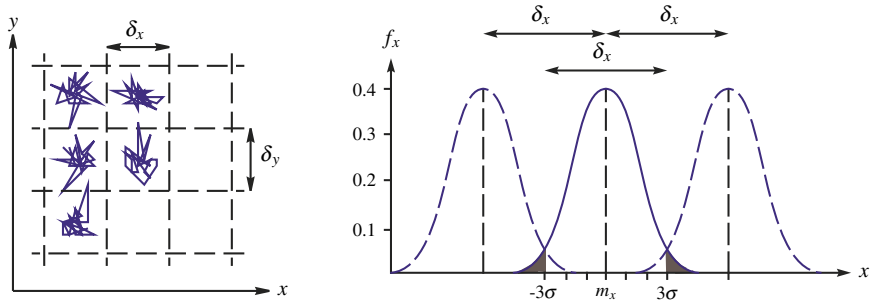

(a) Two dimensional random motion

(b) The probability density functions of three adjacent points on the x-axis

Fig. 1. The random motion of a two-dimensional nanopositioner. The random motion in the x and y-axis is bounded by δ_x and δ_y. In the x-axis, the standard deviation and mean are σ_x and m_x respectively. The shaded areas represent the probability of the position being outside the range specified by δ_x.

of random positioning errors plotted in Fig. 1(a). Observe that the peak-to-peak amplitude of random motion is bounded by δ_x and δ_y, however this range is occasionally exceeded. If the random position variation is assumed to be Gaussian distributed, the probability density functions of three adjacent points, spaced by δ_x, are plotted in Fig. 1(b). In this example, δ_x is equal to $\pm 3\sigma_x$ or $6\sigma_x$, that is, 99.7% of the samples fall within the range specified by δ_x. Restated, there is a 0.3% chance that the position is exceeding δ_x and straying into a neighboring area, this probability is shaded in gray.

For many positioning applications, a 99.7% probability that the position falls within $\delta_x = 6\sigma_x$ is an appropriate definition for the resolution. To be precise, this definition should be referred to as the 6σ-resolution and specifies the minimum spacing between two adjacent points that do not overlap 99.7% of the time. In the following, this definition will be adopted for the resolution of nanopositioning systems.

3. Sources of nanopositioning noise

The three major sources of noise in a nanopositioning systems are the sensor noise, external noise, and the amplifier output voltage noise.

3.1. Sensor noise

The noise characteristics of a position sensor are primarily dependent on the physical method used for detection [13]. Although there are a vast range of sensing techniques available, for the purpose of noise analysis, these can be grouped into two catergories: baseband sensors and modulated sensors.

Baseband sensors involve a direct measurement of position from a physical variable that is sensitive to displacement. Examples include resistive strain sensors, piezoelectric strain sensors and optical triangulation sensors [14,15,13]. The power spectral density of a baseband sensor is typically described by the sum of white noise and $1/f$ noise, where $1/f$ noise has a power spectral density that is inversely proportional to frequency [16,17]. $1/f$ noise is used to approximate the power spectrum of physical processes such as flicker noise in resistors and current noise in transistor junctions. The power spectral density of a baseband sensor $S_{n_s}(f)$ can be written

$$S_{n_s}(f) = A_s \frac{f_{nc}}{|f|} + A_s, \tag{1}$$

where A_s is the mid-band density, expressed in units^2/Hz and f_{nc} is the $1/f$ corner frequency.

Modulated sensors use a high-frequency excitation to detect position. For example, capacitive position sensors, eddy-current sensors, LVDT sensors [14,13]. Although these sensors require a demodulation process that inevitably adds noise, this disadvantage is usually outweighed by the removal or reduction of $1/f$ noise. The power spectral density $S_{n_s}(f)$ of a modulated sensor can generally be approximated by

$$S_{n_s}(f) = A_s, \tag{2}$$

where A_s is the noise density, expressed in units^2/Hz.

3.2. External noise

The external force noise exerted on a nanopositioner is highly dependent on the ambient environmental conditions and cannot be generalized. Typically, the power spectral density consists of broad spectrum background vibration with a number of narrow band spikes at harmonic frequencies of the mains power source and any local rotating machinery. Although the external force noise must be measured in situ, for the purposes of simulation, it is useful to assume a white power spectral density A_w, that is

$$S_w(f) = A_w. \tag{3}$$

Clearly a white power spectral density does not provide an accurate estimate of externally induced position noise. However, it does illustrate the response of the control system to noise from this source.

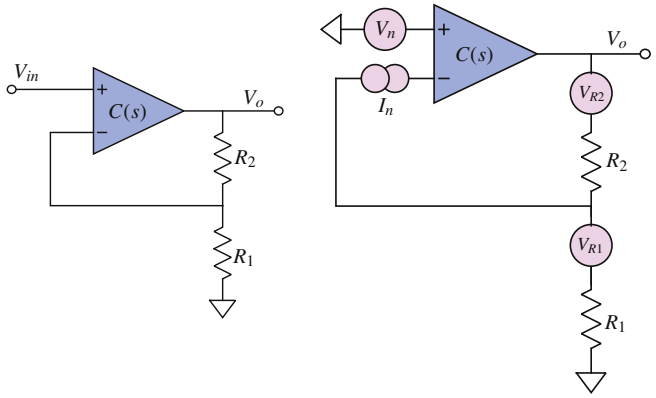

(a) Voltage amplifier

(b) Equivalent noise circuit

Fig. 2. The simplified schematic of a voltage amplifier and its equivalent noise circuit. The noise sources V_n and I_n represent the equivalent input voltage noise and current noise of the amplifier. V_{R1} and V_{R2} are the thermal noise of the feedback resistors.

Please cite this article in press as: Fleming AJ. Measuring and predicting resolution in nanopositioning systems. Mechatronics (2013), http://dx.doi.org/10.1016/j.mechatronics.2013.10.003

3.3. Amplifier noise

The high-voltage amplifier is a key component of any piezoelectric actuated system. It amplifies the control signal from a few volts up to the hundreds of volts required to obtain full stroke from the actuator. For the purpose of noise analysis, the simplified schematic diagram of a non-inverting amplifier in shown in Fig. 2(a). This model is sufficient to represent the characteristics of interest. The opamp represents the differential gain stage and output stage of the amplifier. As high-voltage amplifiers are often stabilized by a dominant pole, the open-loop dynamics can be approximated by a high-gain integrator $C(s) = \alpha_{ol}/s$, where α_{ol} is the open-loop DC gain. With this approximation, the closed-loop transfer function is

$$\frac{V_o}{V_{in}} = \frac{1}{\beta}\frac{\alpha_{ol}\beta}{s + \alpha_{ol}\beta}, \tag{4}$$

where $\beta$is the feedback gain $\frac{R_1}{R_2+R_1}$. The closed-loop DC gain and -3 dB bandwidth are:

$$\text{DC Gain} = \frac{1}{\beta} = \frac{R_2 + R_1}{R_1}, \tag{5}$$

$$\text{Bandwidth} = \alpha_{ol}\beta = \alpha_{ol}\frac{R_1}{R_2 + R_1}\ \text{rad/s}.$$

The random noise of a high-voltage amplifier is dominated by the thermal noise of the feedback resistors and the noise generated by the amplifier circuit that precedes the most gain, which is the differential input stage. These noise processes are illustrated in Fig. 2(b) and are assumed to be Gaussian distributed white noise with spectral density expressed in nV or pA per $\sqrt{\text{Hz}}$. Typical values for the resistances and noise sources are shown in Table 1.

To find the spectral density of the output voltage, the contribution from each source must be computed then square-summed. The equations relating each noise source to the output voltage [18] are collated in Table 2. Also included in Table 2 are the simulated noise values for the example parameters listed in Table 1. Both circuits have a gain of 20 achieved with a 200 kΩ and 10.5 kΩ feedback resistor network. The difference between the two circuits is the choice of transistors in the input differential gain stage of the amplifier. One uses Bipolar Junction Transistors (BJTs) while the other uses Junction Field Effect Transistors (JFETs). While BJTs have a lower noise voltage than JFETs, they also exhibit significant current noise which renders them unsuitable in applications involving large source impedances. As the feedback resistor R_2 in a high-voltage amplifier is typically in the hundreds of kΩor MΩ, the dominant noise process in a BJT circuit is always the current noise I_n. This is observed in the BJT example in Table 2. JFETs are not often used in low-noise applications as they exhibit higher voltage-noise than BJT circuits. However, due to the extremely low current-noise of JFETs and the importance of current-noise in this application, JFETs are preferable.

Table 2 lists the output power spectral densities of the BJT and JFET circuit. To find the total RMS and peak-to-peak noise voltage, the equivalent noise bandwidth of the amplifier can be determined using Table 3. However, the noise power spectral densities of V_n and I_n also exhibit $1/f$ noise or flicker noise, as illustrated in Fig. 3(a).

Table 1
Example noise and resistance parameters for the amplifier shown in Fig. 2. Two cases are considered, one where the differential input stage is constructed from Bipolar Junction Transistors (BJTs) and another where Junction Field Effect Transistors (JFETs) are used.

	BJT circuit	JFET circuit ($\text{nV}/\sqrt{\text{Hz}}$)
V_n	$10\ \text{nV}/\sqrt{\text{Hz}}$	$50\ \text{nV}/\sqrt{\text{Hz}}$
I_n	$10\ \text{pA}/\sqrt{\text{Hz}}$	$0.1\ \text{pA}/\sqrt{\text{Hz}}$
R_1	10.5 kΩ	10.5 kΩ
R_2	200 kΩ	200 kΩ

Table 2
The output voltage noise contributions of the high-voltage amplifier circuit in Fig. 2, where k is Boltzmann's constant (1.38×10^{-23} J/K) and T is the temperature in Kelvin.

Source	V_o	BJT circuit ($\text{nV}/\sqrt{\text{Hz}}$)	JFET circuit ($\text{nV}/\sqrt{\text{Hz}}$)
Voltage noise V_n	$V_n\frac{R_2+R_1}{R_1}$	201	1002
Current noise I_n	I_nR_2	2000	20
R_1 noise = $\sqrt{4kTR_1}$	$\sqrt{4kTR_1}\frac{R_2}{R_1}$	251	251
R_2 noise = $\sqrt{4kTR_2}$	$\sqrt{4kTR_2}$	57	57
Total		2027	1034

Table 3
Equivalent noise bandwidth f_e of some low-order filters with cut-off frequency f_c.

Filter order	f_e
1	$1.57 \times f_c$
2	$1.11 \times f_c$
3	$1.05 \times f_c$
4	$1.025 \times f_c$

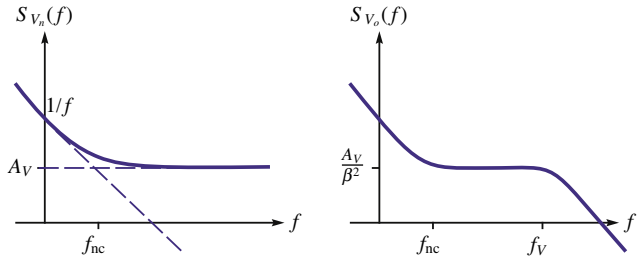

(a) Input voltage noise V_n (b) Output voltage noise V_o

Fig. 3. Power spectral density of the input and output voltage noise of a high-voltage amplifier. f_{nc} is the noise corner frequency.

The noise density in Fig. 3(a) can be described as the sum of a white noise process and $1/f$ noise, that is, the power spectral density can be written

$$S_{V_n}(f) = A_V\frac{f_{\text{nc}}}{|f|} + A_V. \tag{6}$$

where f_{nc} is the noise corner frequency and A_V is the mid-band density, expressed in V^2/Hz.

Since the voltage noise V_n strongly dominates the output noise in this case, the other sources can be readily neglected. The power spectral density of the amplifier output voltage is then approximately

$$S_{V_o}(f) = \left(A_V\frac{f_{\text{nc}}}{|f|} + A_V\right)\frac{1}{\beta^2}\left|\frac{\alpha_{ol}\beta}{j2\pi f + \alpha_{ol}\beta}\right|^2, \tag{7}$$

$$= \frac{A_V}{\beta^2}\left(\frac{f_{\text{nc}}}{|f|} + 1\right)\frac{f_V^2}{f^2 + f_V^2}, \tag{8}$$

where $f_V = \alpha_{ol}\beta/2\pi$ is the closed-loop bandwidth of the amplifier (in Hz) and $1/\beta$ is the DC gain. The power spectral density of the output voltage noise is plotted in Fig. 3(b).

Please cite this article in press as: Fleming AJ. Measuring and predicting resolution in nanopositioning systems. Mechatronics (2013), http://dx.doi.org/10.1016/j.mechatronics.2013.10.003

In addition to the power spectral density, the time-domain variance of the output voltage noise V_o is also of interest. This can be determined directly from the power spectral density,

$$E\left[V_o^2\right] = \frac{A_V}{\beta^2}\int_0^\infty \left(\frac{f_{nc}}{|f|}+1\right)\frac{f_V^2}{f^2+f_V^2} \tag{9}$$

$$= \frac{A_V}{\beta^2}\left(\int_0^\infty \frac{f_{nc}}{|f|}\frac{f_V^2}{f^2+f_V^2}df + \int_0^\infty \frac{f_V^2}{f^2+f_V^2}df\right) \tag{10}$$

In this expression there are two integral terms. The second integral term represents the variance of a first-order filter driven with white noise and can be evaluated using Table 3. The first integral can be evaluated with the following integral pair obtained from [19] (45.3.6.14)

$$\int \frac{1}{f}\frac{1}{bf^2+a}df = \frac{1}{2a}\log\frac{f^2}{bf^2+a}. \tag{11}$$

Rearranging (10) and substituting the result for the second term yields

$$E\left[V_o^2\right] = \frac{A_V}{\beta^2}\left(f_{nc}f_V^2\int_0^\infty \frac{1}{f}\frac{1}{f^2+f_V^2}df + 1.57f_V\right), \tag{12}$$

which can be solved with the integral pair (11) where $a = f_V^2$ and $b = 1$. The result is

$$E\left[V_o^2\right] = \frac{A_V}{\beta^2}\left(\frac{f_{nc}}{2}\log\left[\frac{f^2}{f^2+f_V^2}\right]_0^\infty + 1.57f_V\right). \tag{13}$$

The first term in this equation is problematic as it represents a process with infinite variance which is due to the low-frequency drift associated with $1/f$ noise. In the analysis of devices that exhibit $1/f$ noise, for example opamps, it is preferable to make a distinction between drift and noise. Noise is defined as the varying part of a signal with frequency components above f_L Hz, while drift is defined as random motion below f_L Hz. In nanopositioning applications, a suitable choice for f_L is between 0.01 Hz and 0.1 Hz.

The expression for variance can be modified to include only frequencies above f_L,

$$E\left[V_o^2\right] = \frac{A_V}{\beta^2}\left(\frac{f_{nc}}{2}\log\frac{f_L^2+f_V^2}{f_L^2}+1.57f_V\right). \tag{14}$$

From this equation, two important properties can be observed:

1. The variance is not strongly dependent on f_L so the choice of this parameter is not critical; and
2. The variance is proportional to the noise corner frequency f_{nc}, so this parameter should be minimized at all costs.

For an example of the importance of $1/f$ noise, consider a standard voltage amplifier with a gain of 20, a bandwidth of 2 kHz, an input voltage noise density of 10,000 nV^2/Hz ($100\ nV/\sqrt{Hz}$), and a noise corner frequency of 100 Hz. The total variance of the output voltage noise is 0.0165 mV^2, which is equivalent to an RMS value of 0.13 mV and a peak-to-peak amplitude of 0.77 mV. The $1/f$ noise accounts for 24% of the variance.

If the noise corner frequency is increased by a factor of ten, the peak-to-peak noise approximately doubles to 1.4 mV and the $1/f$ noise now accounts for 76% of the variance. Hence, the noise corner frequency should be kept as low as possible.

Table 4
Summary of the foremost noise sources in a nanopositioning system.

Noise source	Symbol	Power spectral density
Amplifier voltage noise	$S_{V_o}(f)$	$\frac{A_V}{\beta^2}\left(\frac{f_{nc}}{\lvert f\rvert}+1\right)\frac{f_V^2}{f^2+f_V^2}$
Sensor noise	$S_{n_s}(f)$	A_s
External noise	$S_w(f)$	A_w

4. Closed-loop position noise

In the previous section it was concluded that the foremost sources of noise in a nanopositioning application are the amplifier noise, sensor noise and external noise. The spectral densities of these sources is summarized in Table 4. In the following, the closed-loop position noise due to each source is derived.

4.1. Noise sensitivity functions

To derive the closed-loop position noise, the response of the closed-loop system to each noise source must be considered. In particular, we need to specify the location where each source enters the feedback loop. The amplifier noise V_o appears at the plant input. In contrast, the external noise w acts at the plant output, and the sensor noise n_s disturbs the measurement.

A single axis feedback loop with additive noise sources is illustrated in Fig. 4. For the sake of simplicity, the voltage amplifier is considered to be part of the controller. The transfer function from the amplifier voltage noise V_o to the position d is the input sensitivity function,

$$\frac{d(s)}{V_o(s)} = \frac{P(s)}{1+C(s)P(s)}. \tag{15}$$

Likewise, the transfer function from the external noise w to the position d is the sensitivity function,

$$\frac{d(s)}{w(s)} = \frac{1}{1+C(s)P(s)}. \tag{16}$$

Finally, the transfer function from the sensor noise n_s to the position d is the negated complementary sensitivity function,

$$\frac{d(s)}{n_s(s)} = \frac{-C(s)P(s)}{1+C(s)P(s)} \tag{17}$$

4.2. Closed-loop position noise spectral density

With knowledge of the sensitivity functions and the noise power spectral densities, the power spectral density of the position noise due to each source can be derived. The position noise power spectral density due to the amplifier output voltage noise $S_{dV_o}(f)$ is

$$S_{dV_o}(f) = S_{V_o}(f)\left|\frac{d(j2\pi f)}{V_o(j2\pi f)}\right|^2, \tag{18}$$

$$= \frac{A_V}{\beta^2}\left(\frac{f_{nc}}{|f|}+1\right)\frac{f_V^2}{f^2+f_V^2}\left|\frac{d(j2\pi f)}{V_o(j2\pi f)}\right|^2. \tag{19}$$

Similarly, the position noise power spectral density due to the external force noise $S_{dw}(f)$ is

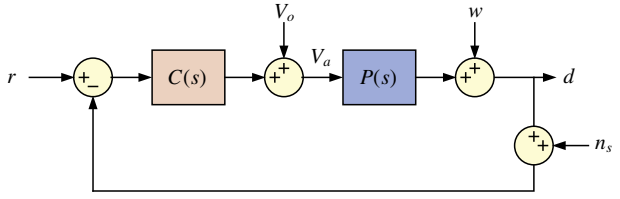

Fig. 4. A single axis feedback control loop with a plant P and controller C. The amplifier voltage noise V_o acts at the plant input while the external noise w effects the actual position and the sensor noise n_s disturbs the measurement. V_a is voltage noise applied to the nanopositioner including the amplifier noise and the filtered sensor noise.

Please cite this article in press as: Fleming AJ. Measuring and predicting resolution in nanopositioning systems. Mechatronics (2013), http://dx.doi.org/10.1016/j.mechatronics.2013.10.003

$$S_{dw}(f) = S_w(f)\left|\frac{d(j2\pi f)}{w(j2\pi f)}\right|^2, \tag{20}$$

$$= A_w\left|\frac{d(j2\pi f)}{w(j2\pi f)}\right|^2. \tag{21}$$

Finally, the position noise power spectral density due to the sensor noise $S_{dn_s}(f)$ is

$$S_{dn_s}(f) = S_{n_s}(f)\left|\frac{d(j2\pi f)}{n_s(j2\pi f)}\right|^2, \tag{22}$$

$$= A_s\left|\frac{d(j2\pi f)}{n_s(j2\pi f)}\right|^2. \tag{23}$$

The total position noise power spectral density $S_d(f)$ is the sum of the three individual sources,

$$S_d(f) = S_{dV_o}(f) + S_{dw}(f) + S_{dn_s}(f). \tag{24}$$

The position noise variance can also be found

$$E\left[d^2\right] = \int_0^\infty S_d(f)df, \tag{25}$$

which is best evaluated numerically. If the noise is Gaussian distributed, the 6σ-resolution of the nanopositioner is

$$6\sigma - \text{resolution} = 6\sqrt{E[d^2]} \tag{26}$$

4.3. Closed-loop noise approximations with integral control

If a simple integral controller is used, $C(s) = \alpha/s$, the transfer functions from the amplifier and external noise to displacement can be approximated by

$$\frac{d(s)}{V_o(s)} = \frac{sP(0)}{s+\alpha P(0)}, \quad \frac{d(s)}{w(s)} = \frac{s}{s+\alpha P(0)}, \tag{27}$$

where $P(0)$ is the DC-Gain of the plant. Likewise, the complimentary sensitivity function can be approximated by

$$\frac{d(s)}{n_s(s)} = \frac{\alpha P(0)}{s+\alpha P(0)}. \tag{28}$$

With the above approximations of the sensitivity functions, the closed-loop position noise power spectral density can be derived. From (19) and (27) the position noise density due to the amplifier voltage noise $S_{dV_o}(f)$ is

$$S_{dV_o}(f) \approx \frac{A_V P(0)^2}{\beta^2}\left(\frac{f_{nc}}{|f|}+1\right)\frac{f_V^2}{f^2+f_V^2}\frac{f^2}{f^2+f_{cl}^2}, \tag{29}$$

where $f_{cl} = \frac{\alpha P(0)}{2\pi}$ is the closed-loop bandwidth. As illustrated in Fig. 5(a), the position noise due to the amplifier has a bandpass characteristic with a mid-band density of $A_V P(0)^2/\beta^2$.

From (21) and (28) the position noise density due to the external noise $S_{dw}(f)$ is

$$S_{dw}(f) \approx A_w\frac{f^2}{f^2+f_{cl}^2}, \tag{30}$$

which has a high-pass characteristic as illustrated in Fig. 5(b) with a corner frequency equal to the closed-loop bandwidth.

The closed-loop position noise due to the sensor $S_{dn_s}(f)$ can be derived from (23) and (28), and is

$$S_{dn_s}(f) \approx A_s\frac{f_{cl}^2}{f^2+f_{cl}^2}, \tag{31}$$

which has a low-pass characteristic with a density of A_s and a corner frequency equal to the closed-loop bandwidth, as illustrated in Fig. 5(c).

The power spectral densities due to each source are plotted in Fig. 5. As the closed-loop bandwidth f_{cl} is increased, the sensor noise contribution also increases. However, a greater closed-loop bandwidth also results in attenuation of the amplifier voltage noise and external force noise. Hence, a lesser closed-loop bandwidth does not necessarily imply a lesser position noise, particularly if the amplifier or external force noise is significant. An important observation is that the amplifier bandwidth f_V should not be unnecessarily higher than the closed-loop bandwidth f_{cl}. In addition, if the sensor induced noise is small compared to the amplifier induced noise, the closed-loop bandwidth should preferably be greater than the noise corner frequency of the voltage amplifier.

4.4. Closed-loop position noise variance

Although the expression for variance (25) is generally evaluated numerically, in some cases it is straightforward and useful to derive analytic expressions. One such case is the position noise variance due to sensor noise ($E[d^2]$due to n_s) when integral control is applied. As demonstrated in the forthcoming examples, sensor noise is typically the dominant noise process in a feedback controlled nanopositioning system. As a result, other noise sources can sometimes by neglected.

As the sensor noise density is approximately constant and the sensitivity function (28) is approximately first-order, the resulting position noise can be determined from Table 3,

$$\sqrt{E[d^2]} \text{ due to } n_s = \sqrt{A_s}\sqrt{1.57 f_{cl}}, \tag{32}$$

The corresponding 6σ-resolution is

$$6\sigma - \text{resolution} = 6\sqrt{A_s}\sqrt{1.57 f_{cl}}. \tag{33}$$

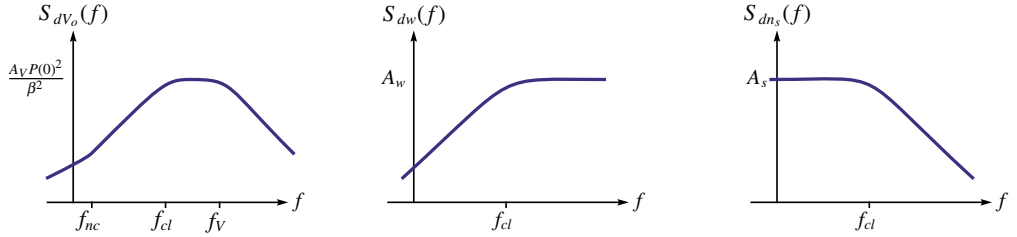

(a) The position noise power spectral density due to amplifier voltage noise $S_{dV_o}(f)$

(b) The position noise power spectral density due to external noise $S_{dw}(f)$

(c) The position noise power spectral density due to sensor noise $S_{dn_s}(f)$

Fig. 5. The position noise power spectral density due to the amplifier voltage noise (a), external disturbance (b) and sensor noise (c). At frequencies lower than the closed-loop bandwidth f_{cl}, the position noise is dominated by the sensor. At higher frequencies, the amplifier noise and external disturbances dominate.

Please cite this article in press as: Fleming AJ. Measuring and predicting resolution in nanopositioning systems. Mechatronics (2013), http://dx.doi.org/10.1016/j.mechatronics.2013.10.003

This expression can be used to determine the minimum resolution of a nanopositioning system given only the sensor noise density and closed-loop bandwidth. It can also be rearranged to reveal the maximum closed-loop bandwidth achievable given the sensor noise density and the required resolution.

$$\text{maximum bandwidth(Hz)} = \left(\frac{6\sigma - \text{resolution}}{7.51\sqrt{A_s}}\right)^2. \tag{34}$$

For example, consider a nanopositioner with integral feedback control and a capacitive sensor with a noise density of 30 pm/$\sqrt{\text{Hz}}$. The maximum bandwidth with a resolution of 1 nm is

$$\text{maximum bandwidth} = \left(\frac{1\times10^{-9}}{7.51\times30\times10^{-12}}\right)^2 = 11\ \text{Hz}$$

4.5. A note on units

In the previous discussion it was been assumed that the nanopositioner model $P(s)$ in Fig. 4 has an output equal to position, preferably in nanometers. In practice however, this signal is the output voltage of a displacement sensor with sensitivity, k V/nm or $1/k$ nm/V. Rather than incorporating an additional gain into the equations above, it is preferable to perform the analysis with respect to the output voltage, then scale the result accordingly.

For example, if a nanopositioner has an output sensor voltage of 1 mV/nm, the noise analysis can be performed to find the spectral density and variance of the sensor voltage. Once the final power spectral density has been found, it can be scaled to nm by multiplying by $1/k^2$, which in this case is $1/(1\times10^{-3})^2$. Alternatively, the RMS value or 6σ-resolution can be found in terms of the sensor voltage then multiplied by $1/k$.

5. Simulation examples

5.1. Integral controller noise simulation

In this section an example nanopositioner is considered with a range of 100 μm at 200 V and a resonance frequency of 1 kHz. The system model is

$$P(s) = 500\frac{\text{nm}}{\text{V}}\times\frac{\omega_r^2}{s^2+2\omega_r\zeta_r s+\omega_r^2}, \tag{35}$$

where $\omega_r = 2\pi1000$ and $\zeta_r = 0.05$. The system includes a capacitive position sensor and voltage amplifier with the following specifications.

- The capacitive position sensor has a noise density of 20 pm/$\sqrt{\text{Hz}}$.
- The voltage amplifier has a gain of 20, a bandwidth of 2 kHz, an input voltage noise density of 100 nV/$\sqrt{\text{Hz}}$, and a noise corner frequency of 100 Hz.

The feedback controller in this example is a simple integral controller with compensation for the sensitivity of the plant, that is

$$C(s) = \frac{1}{500\ \text{nm/V}}\frac{\alpha}{s}, \tag{36}$$

where α is the gain of the controller and also the approximate bandwidth (in rad/s) of the closed-loop system. All of the system parameters are summarized in Table 5.

With the noise characteristics and system dynamics defined, the next step is to compute the spectral density of the position noise due to the amplifier voltage noise, which is

Table 5
Specifications of an example nanopositioning system.

Parameter	Value	Alternate units
Closed-loop bandwidth f_{cl}	50 Hz	
Controller gain α	314	
Amplifier bandwidth f_V	2 kHz	
Amplifier gain $1/\beta$	50	
Amplifier input voltage noise A_V	100 nV/$\sqrt{\text{Hz}}$	10,000 nV^2/Hz
Amplifier output voltage noise	5 μV/$\sqrt{\text{Hz}}$	25 μV^2/Hz
Amplifier noise corner frequency f_{nc}	100 Hz	
Sensor noise A_s	20 pm/$\sqrt{\text{Hz}}$	400 pm^2/Hz
Position range	100 μm	
Sensitivity $P(0)$	500 nm/V	
Resonance frequency ω_r	$2\pi\times10^3$ r/s	1 kHz
Damping ratio ζ_r	0.05	

$$S_{dV_o}(f) = S_{V_o}(f)\left|\frac{d(j2\pi f)}{V_o(j2\pi f)}\right|^2 \tag{37}$$

$$= \frac{A_V}{\beta^2}\left(\frac{f_{\text{nc}}}{|f|}+1\right)\frac{f_V^2}{f^2+f_V^2}\left|\frac{P(j2\pi f)}{1+C(j2\pi f)P(j2\pi f)}\right|^2. \tag{38}$$

The power spectral density of position noise due to the sensor noise can also be found from Eq. (23)

$$S_{dn_s}(f) = S_{n_s}(f)\left|\frac{d(j2\pi f)}{n_s(j2\pi f)}\right|^2 \tag{39}$$

$$= A_s\left|\frac{C(j2\pi f)P(j2\pi f)}{1+C(j2\pi f)P(j2\pi f)}\right|^2. \tag{40}$$

The total density of the position noise can now be calculated from Eq. (24). The total spectral density and its components are plotted in Fig. 6(a). Clearly, the sensor noise is the dominant noise process. This is the case in most nanopositioning systems with closed-loop position feedback.

The variance of the position noise can be determined by solving the integral for variance numerically,

$$\sigma^2 = E\left[d^2\right] = \int_0^\infty S_d(f)df \tag{41}$$

The result is

$$\sigma^2 = 0.24\ \text{nm}^2, \quad \text{or} \quad \sigma = 0.49\ \text{nm},$$

which implies a 6σ-resolution of 2.9 nm.

In systems with lower closed-loop bandwidth, the $1/f$ noise of the amplifier can become dominant. For example, if the closed-loop bandwidth of the previous example is reduced to 1 Hz, the new power spectral density, plotted Fig. 6(b), differs significantly. The resulting variance and standard deviation are

$$\sigma^2 = 0.093\ \text{nm}^2, \quad \text{or} \quad \sigma = 0.30\ \text{nm},$$

which implies a 6σ-resolution of 1.8 nm. Not a significant reduction considering that the closed-loop bandwidth has been reduced to 2% of its previous value. More generally, the resolution can be plotted against a range of closed-loop bandwidths to reveal the trend. In Fig. 7, the 6σ-resolution is plotted against a range of closed-loop bandwidths from 100 mHz to 60 Hz. The curve has a minima of 1.8 nm at 0.4 Hz. Below this frequency, amplifier noise is the major contributor, while at higher frequencies, sensor noise is more significant.

5.2. Noise simulation with inverse model controller

In the previous example, the integral controller does not permit a closed-loop bandwidth greater than 100 Hz. Many other model-based controllers can achieve much better performance. One simple controller that demonstrates the noise characteristics of a model based controller is the combination of an integrator and notch

Please cite this article in press as: Fleming AJ. Measuring and predicting resolution in nanopositioning systems. Mechatronics (2013), http://dx.doi.org/10.1016/j.mechatronics.2013.10.003

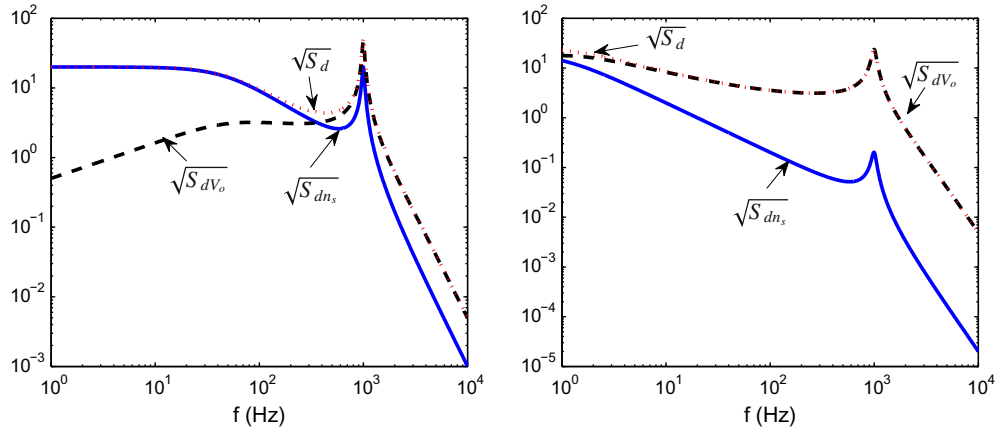

(a) 50 Hz Closed-loop bandwidth (b) 1 Hz Closed-loop bandwidth

Fig. 6. The spectral density of the total position noise $\sqrt{S_d(f)}$ and its two components, the amplifier output voltage noise $\sqrt{S_{dV_o}(f)}$ and sensor noise $\sqrt{S_{dn_s}(f)}$ (all in pm/$\sqrt{\text{Hz}}$). With a 50 Hz bandwidth (a), the total noise is primarily due to the sensor. However, with a lower bandwidth of 1 Hz (b), the noise is dominated by the voltage amplifier.

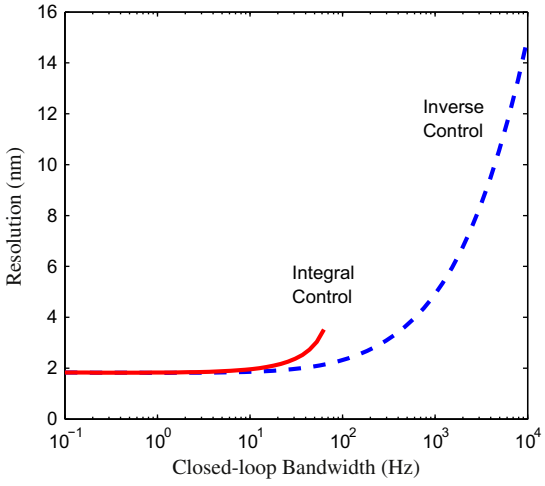

Fig. 7. Resolution of the example nanopositioning system with integral control (solid line) and inverse control (dashed). When the closed-loop bandwidth is less than 10 Hz, the resolution is limited by the amplifier noise. At greater closed-loop bandwidth, the sensor noise becomes dominant. The premature degradation of the integral controller resolution is due to the low gain-margin and resonant closed-loop response.

filter, or direct inverse controller. The transfer function is an integrator combined with an inverse model of the plant,

$$C(s) = \frac{\alpha}{s}\frac{1}{500\ \text{nm/V}}\frac{s^2 + 2\omega_r\zeta_r s + \omega_r^2}{\omega_r}. \tag{42}$$

The resulting loop-gain $C(s)P(s)$ is an integrator, so stability is guaranteed and the closed-loop bandwidth is α rad/s. With such a controller it is now possible to examine the noise performance of feedback systems with wide bandwidth.

Aside from improved bandwidth, the inverse controller also eliminates the resonance peak in the sensor induced noise spectrum. This benefit also occurs with controllers designed to damp the resonance peak [20]. After following the same procedure described in the previous section, the resulting variance for a closed-loop bandwidth of 500 Hz is

$$\sigma^2 = 0.37\ \text{nm}^2, \quad \text{or} \quad \sigma = 0.61\ \text{nm},$$

which implies a 6σ-resolution of 3.7 nm. This is not significantly greater than the 50 Hz controller bandwidth in the previous example, which resulted in a 2.9 nm resolution. When the closed-loop bandwidth of the inverse controller is reduced to 50 Hz, the resolution is 2.1 nm, which is slightly better than the previous example. The difference is due to the absence of the resonance peak in the sensor induced noise.

The resolution of the inverse controller is plotted for a wide range of bandwidths in Fig. 7. The minimum resolution is 1.8 nm at 1 Hz. After approximately 100 Hz, the position noise is due predominantly to the sensor-noise which is proportional to the square-root of closed-loop bandwidth, as described in Eq. (33).

5.3. Feedback versus feedforward control

A commonly discussed advantage of feedforward control systems is the absence of sensor induced noise. However, this view does not take into account the presence of $1/f$ amplifier noise that can result in significant peak-to-peak amplitude.

It is not necessary to derive equations for the noise performance of feedforward systems as this is a special case of the feedback examples already discussed. The positioning noise of a feedforward control system is equivalent to a feedback control system when $C(s) = 0$. Thus, the feedforward controller resolution is the DC resolution of these plots, which in both cases is 2.60 nm.

It is interesting to note that both the integral and inverse controller can achieve slightly less positioning noise than a feedforward control system when the closed-loop bandwidth is very low. This is because the amplifier noise density is greater than the sensor noise density at low frequencies. In the examples considered, the optimal noise performance was achieved with a feedback controller of around 1-Hz bandwidth. A practical system would also require a feedforward input [21].

6. Practical frequency domain noise measurements

The use of a spectrum analyzer to measure noise directly in the frequency domain has many advantages over the time-domain. Firstly, the inputs to a spectrum analyzer are typically equipped with dynamic signal scaling so that low amplitude signals can easily be dealt with. Secondly, spectrum analyzers record a very large amount of low-information data, and through averaging and Fourier transformation, create a small amount of high-information data. If a spectrum analyzer is not available, a signal's spectrum can also be estimated from time domain recordings.

Please cite this article in press as: Fleming AJ. Measuring and predicting resolution in nanopositioning systems. Mechatronics (2013), http://dx.doi.org/10.1016/j.mechatronics.2013.10.003

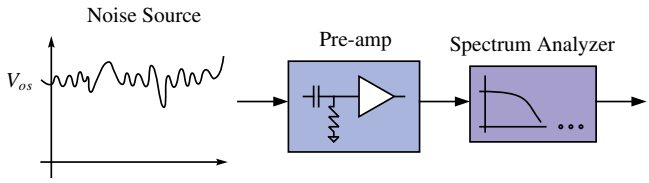

Fig. 8. A frequency domain noise measurement with a preamplifier and spectrum analyzer.

6.1. Preamplification

As the amplitude of a typical noise signal is too small to be applied directly to a spectrum analyzer, it must first be amplified. The signal-path of a noise measurement experiment is illustrated in Fig. 8. A low-noise preamplifier is used between the noise signal and spectrum analyzer. Its purpose is to remove offset voltage and to amplify the signal from microvolts or millivolts to around 100 mV RMS or greater.

To remove the offset voltage and low-frequency drift, an AC-coupled preamplifier uses a first-order high-pass filter to eliminate the DC component of the signal. However, AC-coupling in some instruments implies a cut-off frequency of up to 20 Hz. This is intolerably high in nanopositioning applications where the cut-off frequency should be less than 0.1 Hz. Noise components with frequency less that 0.01 Hz are usually referred to as drift and are not considered here. Most specialty low-noise preamplifiers have the provision for a low-frequency high-pass filter, for example, the Stanford Research SR560 low-noise amplifier has a high-pass cut-off frequency of 0.03 Hz.

When utilizing low-frequency filters, it is important to allow the transient response of the filter to decay before recording data. When measuring small AC signals with large DC components, it may take in excess of 20 time-constants for the transient response to become negligible. With an AC coupling frequency of 0.03 Hz, the required delay is approximately 100 s. More generally, the measurement delay T_D should be at least

$$T_D = \frac{20}{2\pi f_c} \tag{43}$$

where f_c is the high-pass filter cut-off.

6.2. Optimizing the performance of a spectrum analyzer

When using a spectrum analyzer to record power spectral density, the instrument collects each segment individually then updates a running average of the estimate. This is convenient as it avoids the need to record a large amount of time-domain data. It also allows the user to assess the variance of the data in real time which is a simple method for deciding how long to run the experiment.

Regardless of the window function used, the finite data length of each segment results in windowing distortion. This distortion is most evident near 0 Hz where it is convolved with the offset of the signal. The frequency width of windowing distortions can be reduced by increasing the number of samples in each segment. However, this also increases the data lengths and requires more averaging cycles. Low-frequency data points that exhibit windowing artifacts should be removed.

The Fast Fourier transform is defined at uniformly spaced frequencies, this emphasizes higher frequencies when plotted on a logarithmic scale. When studying the spectra of linear systems, logarithmically spaced frequencies are preferred. To approximate this, a wide bandwidth spectral measurement can be split into a number of one or two decade bands.

Typical spectrum analyzers provide a wide range of options for the measurement unit. The units of $V/\sqrt{Hz}$ or V^2/Hz are recommended. The RMS Voltage (Vrms) should be used for noise measurements.

When measuring the power spectral density with a dynamic signal analyzer, it is important to note whether the data is a double-sided or single-sided spectrum and perform a conversion if necessary. The single-sided spectrum is utilized in this work.

7. Experimental demonstration

In this section, an example noise analysis is performed on the piezoelectric tube scanner described in Fig. 9 and Ref. [22]. The frequency response is plotted in Fig. 10. The goal is to quantify the achievable resolution as a function of closed-loop bandwidth.

The voltage amplifier used to drive the tube is a Nanonis HVA4 high-voltage amplifier with a gain of 40. To measure the noise, the amplifier input was grounded and the output was amplified by 1000 using an SR560 preamplifier. To remove DC offset, the input of the preamplifier was AC-coupled with a 0.03 Hz cut-off frequency.

The sensor under consideration is an ADE Tech 4810 Gaging Module with 2804 capacitive sensor, which has a full range of ±100 μm and a sensitivity of 0.1 V/μm. To measure the noise, the sensor is mounted inside an Aluminum block with a flat-bottomed hole and grub screws to secure the probe.

The spectral density of each noise source was recorded with an HP 35670A dynamic signal analyzer. Two frequency ranges were used, one from 0 to 12.5 Hz with 400 points to capture low-frequency noise, and another from 0 Hz to 1.6 kHz with 1600 points. An acceptable measurement variance was achieved with 100 averages for the low-frequency range and 700 averages for the high-frequency range. After exporting the data in $V/\sqrt{Hz}$, the two data sets were concatenated in Matlab. Windowing distortions at DC were removed by truncating the first five frequency points of the low-frequency measurement.

The spectral density of the amplifier was measured to be approximately 1 $\mu V/\sqrt{Hz}$ with a $1/f$ corner frequency of 3 Hz. The resulting open-loop position noise is found using Eq. (18) and the frequency response plotted in Fig. 10. The position noise spectral densities due to the amplifier and sensor are plotted in Fig. 11(a) and (b). Above the $1/f$ corner frequency of 2 Hz, the noise density of the sensor is approximately 25 $pm/\sqrt{Hz}$, which is significantly greater than the noise due to the voltage amplifier.

With knowledge of the voltage and sensor noise, the closed-loop positioning noise can be computed. For the sake of demonstration, an inverse controller similar to that used previously is considered. This is representative of a wide range of model-based controllers. The controller transfer function is,

$$C(s) = \frac{\alpha}{s}\frac{1}{P(s)}, \tag{44}$$

where $P(s)$ is the nanopositioner response plotted in Fig. 10. The sensitivity functions and position noise density due to each source are computed from Eqs. (27) and (28). The resolution is then be found from Eqs. (24)–(26).

In Fig. 12 the closed-loop positioning resolution is plotted against closed-loop bandwidth, which is equal to $\alpha/2\pi$. The minima of 0.5 nm occurs at 0 Hz which implies that feedforward would results in the least positioning noise. In closed-loop, the positioning resolution becomes greater than twice the open-loop noise at frequencies greater than 15 Hz. At higher frequencies, the resolution increases proportional to the square-root of closed-loop bandwidth.

Please cite this article in press as: Fleming AJ. Measuring and predicting resolution in nanopositioning systems. Mechatronics (2013), http://dx.doi.org/10.1016/j.mechatronics.2013.10.003

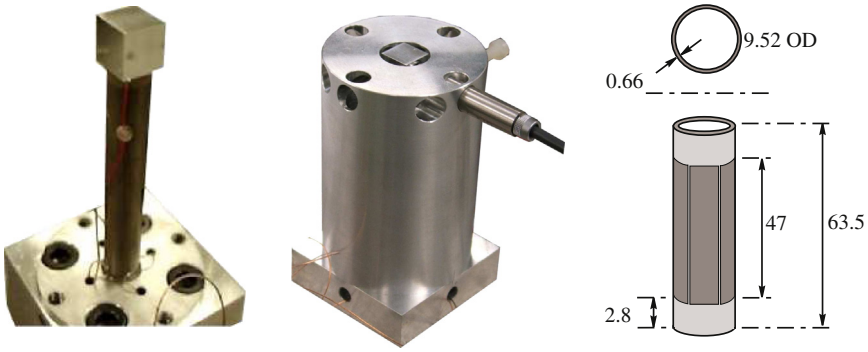

(a) Piezo tube (b) Inside enclosure (c) Dimensions (mm)

Fig. 9. A piezoelectric tube scanner. The tube tip deflects laterally when an electrode is driven by a voltage source. The sensitivity is 171 nm/V which implies a range of approximately 68 μm with a ±200 V excitation. In (b) a capacitive sensor is mounted perpendicular to the cube mounted on the tube tip.

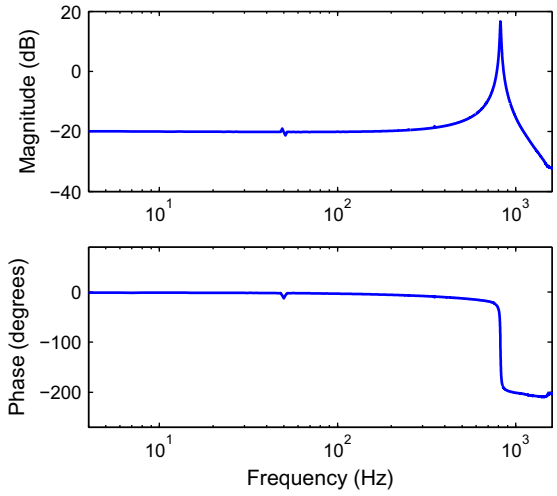

Fig. 10. The lateral frequency response (in μm/V) of the piezoelectric tube scanner pictured in Fig. 9. The response was measured from the applied actuator voltage to the resulting displacement.

This experiment confirms an observation of scanning probe microscope users: Although large range piezoelectric tubes are suitable for atomic force microscopy, they cannot be used for scanning tunneling microscopy where atomic resolution is required. For such experiments, much smaller piezoelectric tubes are used with a travel range of typically 1 μm. This reduces the effect of amplifier voltage noise leading to an improvement in resolution.

8. Time domain noise measurements

As an alternative to frequency domain recording, the position noise can also be estimated directly from time-domain measurements. This procedure involves measuring the amplifier and sensor noise and filtered by the noise sensitivity functions. Compared to frequency-domain techniques, the time-domain approach has a number of benefits: simplicity; a spectrum analyzer is not required; the distribution histogram can be plotted directly; and no assumptions about the distribution are required to estimate the peak-to-peak value or 6σ-resolution. However, there are also a number of disadvantages: it may be difficult to record signals with $1/f$ noise due to their high dynamic range; capturing both low- and high-frequency noise requires data sets; there is less insight into the nature of the noise; it is more difficult to plot the resolution versus bandwidth.

8.1. Total integrated noise

A common method for reporting time-domain noise is known as the total integrated noise, which is the RMS value or standard deviation over a particular measurement bandwidth. The main benefit of total integrated noise is that it can be measured directly using simple instruments. For example, the plot in Fig. 13 can be constructed with a variable cut-off low-pass filter and RMS measuring instrument. The filter order should generally be greater than three to minimize errors resulting from the non-ideal response.

8.2. Estimating the position noise

The most straight-forward and conclusive method for measuring the positioning noise of a nanopositioning system is to measure it directly. However, this approach is not often possible as an additional sensor is required with lower noise and a significantly higher bandwidth than the closed-loop system. In such cases, the position noise can be predicted from measurements of the amplifier and sensor noise. A benefit of this approach is that the closed-loop noise can be predicted for a number of different bandwidths and controllers, much like frequency domain techniques.

Referring to the feedback diagram in Fig. 4, the signals of interest are the amplifier noise V_o and the sensor noise n_s. As the position noise is calculated by superposition, the amplifier noise should be measured with the input signal grounded and the output connected to the nanopositioner. Conversely, the sensor noise should be measured with a dedicated test-rig to avoid the influence of external disturbances. If the sensor noise must be measured in situ, all of the nanopositioner actuators should be disconnect from their sources and short-circuited.

After the constituent noise sources have been recorded, the position noise can be predicted by filtering the noise signals by the sensitivity functions of the control-loop. That is, the position noise is

$$d(t) = n_s(t)\frac{-C(s)P(s)}{1+C(s)P(s)} + V_o(t)\frac{P(s)}{1+C(s)P(s)}. \tag{45}$$

The RMS value of the position noise can now be computed and plotted for a range of different controller-gains and closed-loop bandwidths.

Although the data sizes in time domain experiments must be necessarily large to guarantee statistical validity, this is not a serious impediment since a range of numerical tools are readily available for extracting the required information.

Please cite this article in press as: Fleming AJ. Measuring and predicting resolution in nanopositioning systems. Mechatronics (2013), http://dx.doi.org/10.1016/j.mechatronics.2013.10.003

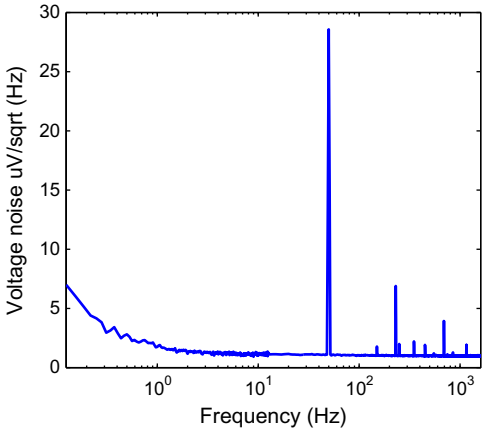

(a) Spectral density of the amplifier voltage noise $\sqrt{S_{V_o}(f)}$ in μV/ $\sqrt{\text{Hz}}$

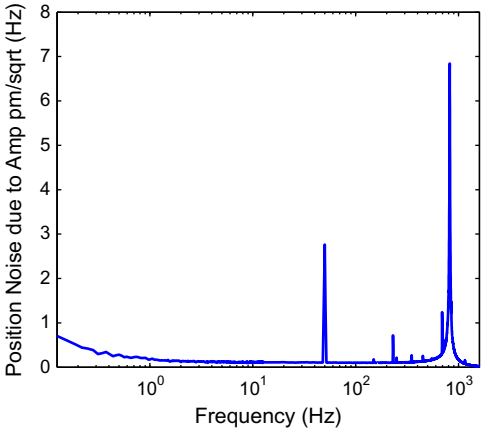

(b) Spectral density of the displacement noise due to the amplifier $\sqrt{S_{dn_s}(f)}$ in pm/ $\sqrt{\text{Hz}}$

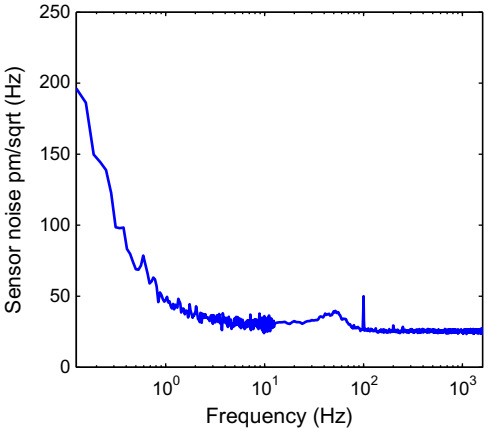

(c) Spectral density of the sensor noise $\sqrt{S_{n_s}(f)}$ in pm/ $\sqrt{\text{Hz}}$

Fig. 11. The spectral density of the amplifier noise, the position noise due to the amplifier, and the sensor noise. In this case, the sensor noise is significantly larger than the amplifier noise.

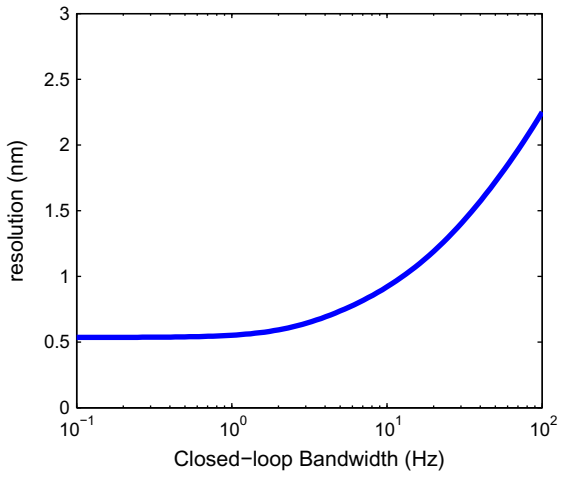

Fig. 12. The experimental 6σ-resolution of the nanopositioner versus closed-loop bandwidth. The best resolution is 0.5 nm which degrades rapidly when the closed-loop bandwidth is increased above 15 Hz.

8.3. Practical considerations

Many of the considerations for frequency domain noise measurements are also valid for time domain measurements. Of particular importance is the need for preamplification and the removal of offset voltages. After a suitable preamplification scheme has been implemented, the position noise can be estimated from recordings of the sensor and amplifier noise. This requires a choice of the recording length and sampling rate. The length of each recording is defined by the lowest spectral component under consideration. WIth a lower frequency limit of 0.1 Hz, a record length of at least ten times the minimum period is required to obtain a statistically meaningful estimate of the RMS value, which implies a minimum recording length of at least 100 s. A longer record length is preferable, but usually not practical.

A more rigorous method for selecting the record length is to calculate the estimator variance as a function of the record length. This relationship was described in [23], however, assumptions are required about the autocorrelation or power spectral density. In most cases, the simple rule-of-thumb discussed above is sufficient.

When selecting the sampling rate, the highest significant frequency that influences position noise should be considered. Since

Please cite this article in press as: Fleming AJ. Measuring and predicting resolution in nanopositioning systems. Mechatronics (2013), http://dx.doi.org/10.1016/j.mechatronics.2013.10.003

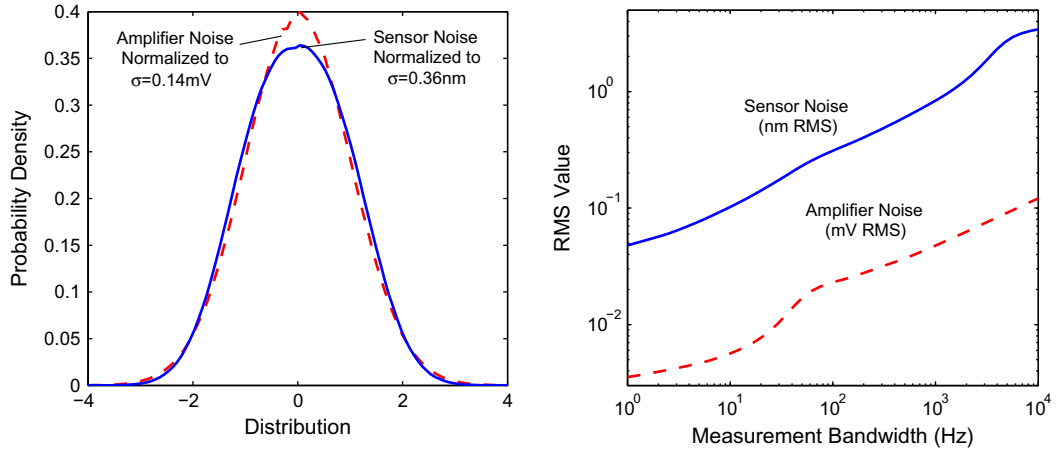

(a) Probability density function (b) RMS Value vs. measurement bandwidth

Fig. 13. The distribution and total integrated noise of the voltage amplifier and capacitive sensor. Both of the sensors exhibit an approximately Gaussian distribution.

Table 6
Recommended parameters for time domain noise recordings.

Record length	100 s
Amplifier bandwidth	f_V
Anti-aliasing filter cut-off frequency	$7.5 \times f_V$
Sampling rate	$15 \times f_V$

the sensor noise is low-pass filtered by the closed-loop response of the control loop, the highest significant frequency is usually the bandwidth of the voltage amplifier. An appropriate choice of sampling rate is fifteen times the amplifier bandwidth. This allows a non-ideal anti-aliasing filter to be utilized with a cut-off frequency of five times the amplifier bandwidth. Since the noise power of a first-order amplifier drops to 3.8% at five times the bandwidth, this technique captures the majority of noise power. The recommended parameters for time-domain noise recordings are summarized in Table 6.

8.4. Experimental demonstration

In this section, the frequency domain noise analysis is repeated in the time domain. The same piezoelectric tube nanopositioner, capacitive sensor and high-voltage amplifier are used. Since the bandwidth of the high-voltage amplifier is 2 kHz, the sampling rate is chosen to be 30 kHz. To remove the DC offset, the high-pass cut-off of the preamplifier was set to 0.1 Hz. The preamplifier is also used for anti-aliasing with a cut-off frequency of 10 kHz as recommended in Table 6. With a record length of 100 s, the data contains 3×10^6 samples.

The distribution and total integrated noise of the voltage amplifier and sensor are plotted in Fig. 13. The RMS value of the amplifier noise is 0.14 mV over the 0.1 Hz to 10 kHz measurement bandwidth which corresponds to a predicted 6σ-resolution of 0.84 mV. The measured 6σ-resolution was 0.86 mV which supports the assumption of approximate Gaussian distribution.

The RMS noise and 6σ-resolution of the capacitive sensor was measured to be 3.6 nm and 20 nm respectively. The capacitive sensor also exhibits an approximately Gaussian distribution, albeit with a slightly greater dispersion than the voltage amplifier.

For the sake of comparison, an inverse controller is used. That is,

$$C(s) = \frac{\alpha}{s}\frac{1}{P(s)}, \tag{46}$$

where $P(s)$ is the second-order model of the nanopositioner and α is the closed-loop bandwidth. The position noise can now be simulated using the noise recordings and Eq. (45).

At low closed-loop bandwidth, the transient response time of the system is significant. For this reason, only the second half of the simulated output is used to calculate the resolution. For the same reason, it is not practical to simulate a closed-loop bandwidth of less than 1 Hz. This is an additional disadvantage of time-domain approaches.

The predicted resolution is plotted against closed-loop bandwidth in Fig. 14. As expected, this plot closely resembles Fig. 12 which was obtained from frequency domain data. The time and frequency domain results are compared below in Table 7. With a closed-loop bandwidth of 100 Hz, the predictions are identical, however, at low closed-loop bandwidth, some discrepancy exists. This is due to the long transient response in the time domain which tends to underestimate the positioning noise. If necessary, a more accurate result can be achieved by significantly increasing the recording length, however this is not usually desirable or practical.

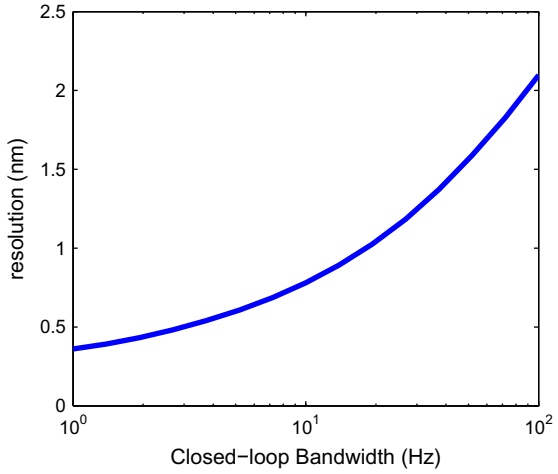

Fig. 14. The 6σ-resolution versus closed-loop bandwidth derived from time-domain measurements. This plot closely matches the frequency-domain result in Fig. 12 except when the closed-loop bandwidth is less than 10 Hz, at these frequencies the time-domain technique underestimates noise.

Please cite this article in press as: Fleming AJ. Measuring and predicting resolution in nanopositioning systems. Mechatronics (2013), http://dx.doi.org/10.1016/j.mechatronics.2013.10.003

Table 7
The predicted closed-loop resolution using frequency and time-domain measurements.

Bandwidth (Hz)	Frequency domain (nm)	Time domain (nm)
100	2.2	2.1
10	0.92	0.78
1	0.55	0.36

9. A simple method for measuring the resolution of nanopositioning systems

The previous time and frequency domain approaches for noise analysis can provide a detailed prediction of resolution versus the closed-loop bandwidth. However, these techniques also require careful measurement practices, specialized equipment, and involved processing of the measured data. Given these complexities, there is a need for a simple practical procedure to accurately estimate the closed-loop resolution of a nanopositioning system. A new procedure that fulfills this goal is described in the following. The method is based on a measurement of the closed-loop steady-state voltage produced by the high-voltage amplifier. The voltage is filtered by the open-loop response of the plant to reveal the closed-loop resolution.

As shown in Fig. 4 the position d is equal to the voltage V_a filtered by the plant model. Hence, the position noise can be estimated by measuring the closed-loop voltage noise V_a and filtering it by the plant dynamics. This measurement can be performed in the time or frequency domain, is straight-forward, and does not require any additional sensors.

The preamplification requirements discussed previously are also applicable here. A preamplifier is required with a gain of approximately 1000 and an AC coupling frequency of 0.1 Hz or less. A simple protection circuit may also be required to avoid exceeding the voltage range of the preamplifier.

In the case of a time-domain recording, the sampling rate should be greater than fifteen times the amplifier bandwidth and the record length should be 100 s or more. The actual position noise can be estimated by filtering the recording by a model of the plant. The portion of the simulated displacement that is effected by the transient response should be excised before calculating the RMS value and resolution.

In the frequency domain, the measured spectrum should be split into two or three decades to provide sufficient resolution and range. For example: 0–12 Hz, 12 Hz to 1.2 kHz, and 1.2–12 kHz. The data should preferably be recorded in units of $V/\sqrt{Hz}$ and have a frequency range of at least five times the amplifier bandwidth. The RMS value and 6σ-resolution can then be found by evaluating the integral

$$\sigma = \int_0^\infty \sqrt{S_{V_a}(f)}|P(j2\pi f)|df \tag{47}$$

where $\sqrt{S_{V_a}(f)}$ is the spectral density of V_a.

In the following, the 'applied voltage' technique is used to estimate the resolution of the piezoelectric tube nanopositioner described in Fig. 9. A simple analog integral controller is used to provide a closed-loop bandwidth of 10 Hz. After setting the reference input to zero, the voltage applied to the nanopositioner was preamplified by an SR560 amplifier with a gain of 500 and an AC coupling frequency of 0.03 Hz. This signal was recorded for 100 s with a sampling rate of 30 kHz.

To estimate the closed-loop positioning noise, the noise recording was filtered by a model of the plant. The distribution of the displacement estimate is plotted in Fig. 15(a) and has an RMS value of 0.24 nm and a 6σ resolution of 1.4 nm. Since 1.4 nm is greater than 6×0.24 nm, the distribution is slightly more dispersed than a Gaussian distribution. The estimated displacement noise can also be used to visualize the expected two-axis performance. In Fig. 15(b), nine 100 ms data sets were taken randomly from the estimated position noise and plotted on a constellation diagram with a spacing equal to the prescribed resolution. The 6σ definition of resolution can be observed to be a true prediction of the minimum reasonable spacing between two distinct points.

10. Techniques for improving resolution

The obvious methods for improving resolution include reducing the noise density and corner frequency of the amplifier and sensor noise, however, these parameters may be fixed. In Section 4.3 is was observed that the amplifier bandwidth should not be unnecessarily greater than the closed-loop bandwidth. Since a piezoelectric actuator is primarily capacitive, the bandwidth can be arbitrarily reduced by installing a resistor in series with the load. The resulting first-order cut-off frequency is $f_c = 1/(2\pi RC)$. This simple tech-

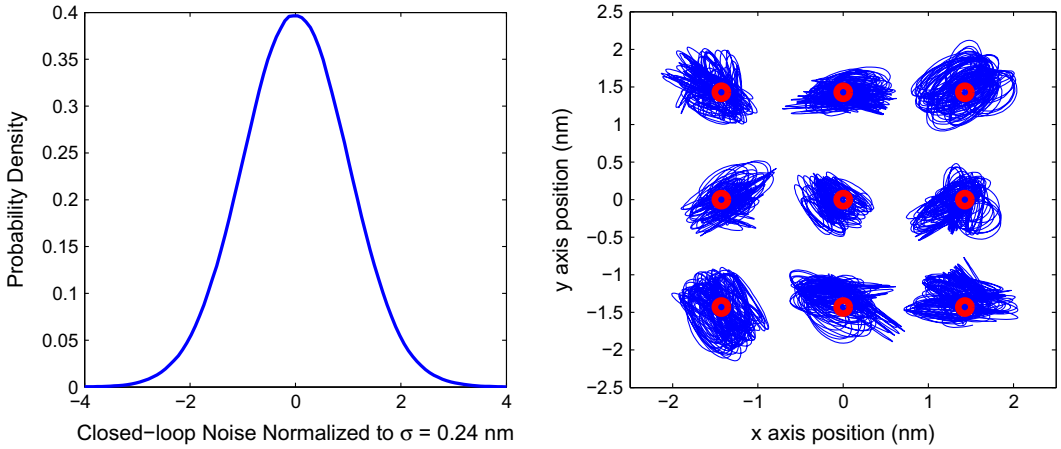

(a) Distribution of the predicted noise

(b) Constellation diagram of nine two-dimensional points spaced by the measured 6σ-resolution.

Fig. 15. The distribution of position noise in a piezoelectric tube nanopositioner with a closed-loop bandwidth of 10 Hz is shown in (a). The standard deviation is 0.24 nm and the 6σ-resolution is 1.4 nm. A time domain recording of the position noise is illustrated in (b) where the red dots are spaced by the 6σ-resolution. The 6σ definition of resolution is observed to be an accurate measure of the minimum distance between two non-overlapping points. (For interpretation of the references to color in this figure legend, the reader is referred to the web version of this article.)

Please cite this article in press as: Fleming AJ. Measuring and predicting resolution in nanopositioning systems. Mechatronics (2013), http://dx.doi.org/10.1016/j.mechatronics.2013.10.003

nique can be used to restrict the bandwidth and avoid unnecessary high frequency noise that may excite uncontrolled mechanical resonances.

A significant source of positioning noise is the excitation of mechanical resonance due to sensor noise. If the mechanical resonance is lightly damped, it may become the dominant noise contributor. This limitation can be aleviated through the use of model-based [24,25] or inverse controllers. However, notch filters and inverse controllers are sensitive to variations in resonance frequency [26,27]. Damping control is an alternative technique that provides improved robustness. Suitable damping controllers for nanopositioning applications include polynomial based control [28], shunt control [29,30], resonant control [31], Force Feedback [12,32], and Integral Resonance Control (IRC) [33,34].

The resolution can also be improved by reducing the closed-loop bandwidth, which may be possible if a feedforward controller is used to compensate for the reduction of servo bandwidth [21,35–37]. The noise sensitivity can also be reduced if the reference trajectory is periodic, which commonly occurs in nanopositioning applications [38]. Periodic trajectories can be effectively controlled using repetitive [39] or iterative controllers [40,41], both of which provide excellent tracking performance with less noise than a standard control loop with similar tracking error.

Further noise advantages can be achieved if the reference trajectory is also narrowband. For example, AFM scan trajectories can be spiral [42,43] or sinusoidal [44–46]. In such cases, the controller bandwidth can be essentially reduced to a single, or a small number of frequencies [31].

Multiple sensors can also be used collaboratively to provide both high resolution and wide bandwidth. For example, a low-noise piezoelectric sensor can be used for active resonance damping while a capacitive sensor is used for low-frequency tracking [47,12]. Magnetoresistive sensors have also shown promise for low-noise high-bandwidth position sensing [48,49]. Multiple sensors can be combined by complementary filters [12] or by an optimal technique in the time [50] or frequency domain [51].

11. Conclusions

In this article the resolution of a nanopositioning system is defined as the minimum distance between two non-overlapping locations. This is equivalent to the maximum peak-to-peak random variation in position. In nanopositioning applications, an appropriate definition of the peak-to-peak variation is the bound that encloses 99.7% of observations. If the contributing noise sources are Gaussian random processes, the peak-to-peak variation is equal to six times the standard deviation, which is referred to as the 6σ-resolution.

The foremost noise sources in a nanopositioning system were identified as the amplifier voltage noise and the displacement sensor noise. The simulation examples demonstrate that the minimum positioning noise usually occurs in open-loop or with very low closed-loop bandwidth. This implies that combined feedback and feedforward control can achieve the best positioning resolution.

Both frequency and time-domain techniques were described for measuring and predicting the closed-loop resolution of a nanopositioning system. Although frequency domain techniques provide a more intuitive understanding of the noise sources, time domain recordings may be easier to perform. In practice, both techniques require careful experimental procedures to avoid underestimating or biasing the results.

Although the frequency and time domain techniques discussed can predict the resolution of any closed-loop system, this process may be too involved for some applications. The 'applied voltage' technique requires only one recording and one filtering operation to predict the closed-loop resolution. Experimental results demonstrate an excellent correlation with other standard methods.

Acknowledgements

This work was supported by the Australian Research Council (DP0986319) and the Center for Complex Dynamic Systems and Control.

References

[1] Devasia S, Eleftheriou E, Moheimani SOR. A survey of control issues in nanopositioning. IEEE Trans Contr Syst Technol 2007;15(5):802–23.
[2] Salapaka SM, Salapaka MV. Scanning probe microscopy. IEEE Contr Syst 2008;28(2):65–83.
[3] Dufrêne YF. Towards nanomicrobiology using atomic force microscopy. Nature Rev Microbiol 2008;6:674–80.
[4] Jalili N, Laxminarayana K. A review of atomic force microscopy imaging systems: application to molecular metrology and biological sciences. Mechatronics 2004;14(8):907–45.
[5] Abramovitch DY, Andersson SB, Pao LY, Schitter G. A tutorial on the mechanisms, dynamics, and control of atomic force microscopes. In: Proc American control conference, New York City, NY; 2007. p. 3488–502.
[6] Mishra S, Coaplen J, Tomizuka M. Precision positioning of wafer scanners. Segmented iterative learning control for nonrepetitive disturbances. IEEE Contr Syst 2007;27(4):20–5. http://dx.doi.org/10.1109/MCS.2007.384130.
[7] Ferreira A, Mavroidis C. Virtual reality and haptics for nanorobotics. IEEE Robot Automat Mag 2006;13(3):78–92.
[8] Tseng AA, editor. Nanofabrication: fundamentals and applications. Singapore: World Scientific; 2008.
[9] Sebastian A, Pantazi A, Pozidis H, Eleftheriou E. Nanopositioning for probe-based data storage. IEEE Contr Syst 2008;28(4):26–35.
[10] Fan Z-Q, Li X-W, Liu Y, Meng Q-G, Wang Y-P, Hou Y-P, et al. Piezo-assisted In Vitro fertilization of mouse oocytes with spermatozoa retrieved from epididymides stored at 4 °C. J Reproduct Develop 2008;54(2):107–12.
[11] Hassen SZS, Heurs M, Huntington EH, Petersen IR, James MR. Frequency locking of an optical cavity using linear-quadratic gaussian integral control. J Phys B: Atom Mol Opt Phys 2009;42(17):175501.
[12] Fleming AJ. Nanopositioning system with force feedback for high-performance tracking and vibration control. IEEE Trans Mech 2010;15(3):433–47.
[13] Fleming AJ. A review of nanometer resolution position sensors: operation and performance. Sensor Actuator A: Phys 2013;190:106–26.
[14] Nyce DS. Linear position sensors. Theory and application. Hoboken (NJ): John Wiley and Sons; 2004.
[15] Fraden J. Handboook of modern sensors: physics, designs, and applications. New York: Springer; 2004.
[16] van Etten WC. Introduction to noise and random processes. West Sussex, England: John Wiley and Sons; 2005.
[17] Brown RG, Hwang PYC. Introduction to random signals and applied kalman filtering. Hoboken (NJ): John Wiley and Sons; 1997.
[18] Horowitz P, Hill W. The art of electronics. Cambridge (UK): Cambridge University Press; 1989.
[19] Poularikas AD. The handbook of formulas and tables for signal processing. Boca Raton (FL): CRC Press; 1999.
[20] Fleming AJ, Aphale SS, Moheimani SOR. A new method for robust damping and tracking control of scanning probe microscope positioning stages. IEEE Trans Nanotechnol 2010;9(4):438–48. http://dx.doi.org/10.1109/TNANO.2009.2032418.
[21] Leang KK, Zou Q, Devasia S. Feedforward control of piezoactuators in atomic force microscope systems. IEEE Contr Syst 2009;29(1):70–82.
[22] Maess J, Fleming AJ, Allgöwer F. Simulation of dynamics-coupling in piezoelectric tube scanners by reduced order finite element models. Rev Sci Instrum 2008;79:015105. http://dx.doi.org/10.1063/1.2826428. 1–9.
[23] Fleming AJ, Moheimani SOR. Adaptive piezoelectric shunt damping. IOP Smart Mater Struct 2003;12(1):18–28.
[24] Salapaka S, Sebastian A, Cleveland JP, Salapaka MV. High bandwidth nano-positioner: a robust control approach. Rev Sci Instrum 2002;75(9):3232–41.
[25] Sebastian A, Salapaka S. Design methodologies for robust nano-positioning. IEEE Trans Contr Syst Technol 2005;13(6):868–76. http://dx.doi.org/10.1109/TCST.2005.854336.
[26] Leang KK, Devasia S. Feedback-linearized inverse feedforward for creep, hysteresis, and vibration compensation in AFM piezoactuators. IEEE Trans Contr Syst Technol 2007;15(5):927–35.
[27] Abramovitch DY, Hoen S, Workman R. Semi-automatic tuning of PID gains for atomic force microscopes. In: Proc American control conference, Seattle, WA; 2008. p. 2684–9.
[28] Aphale SS, Bhikkaji B, Moheimani SOR. Minimizing scanning errors in piezoelectric stack-actuated nanopositioning platforms. IEEE Trans Nanotechnol 2008;7(1):79–90.

[29] Fleming AJ, Moheimani SOR. Sensorless vibration suppression and scan compensation for piezoelectric tube nanopositioners. IEEE Trans Contr Syst Technol 2006;14(1):33–44.
[30] Fleming AJ, Behrens S, Moheimani SOR. Optimization and implementation of multi-mode piezoelectric shunt damping systems. IEEE/ASME Trans Mech 2002;7(1):87–94.
[31] Sebastian A, Pantazi A, Moheimani SOR, Pozidis H, Eleftheriou E. A self servo writing scheme for a MEMS storage device with sub-nanometer precision. In: Proc IFAC world congress, Seoul, Korea; 2008. p. 9241–7.
[32] Fleming AJ, Leang KK. Integrated strain and force feedback for high performance control of piezoelectric actuators. Sensor Actuator A 2010;161(1–2):256–65. http://dx.doi.org/10.1016/j.sna.2010.04.008.
[33] Aphale SS, Fleming AJ, Moheimani SOR. Integral resonant control of collocated smart structures. IOP Smart Mater Struct 2007;16:439–46. http://dx.doi.org/10.1088/0964-1726/16/2/023.
[34] Bhikkaji B, Moheimani SOR. Integral resonant control of a piezoelectric tube actuator for fast nanoscale positioning. IEEE/ASME Trans Mech 2008;13(5):530–7.
[35] Clayton GM, Tien S, Leang KK, Zou Q, Devasia S. A review of feedforward control approaches in nanopositioning for high-speed, SPM. J Dynam Syst Measure Contr 2009;131:061101. 1–19.
[36] Eielsen AA, Gravdahl JT, Pettersen KY. Adaptive feed-forward hysteresis compensation for piezoelectric actuators. Rev Sci Instrum 2012;83(8):085001. http://dx.doi.org/10.1063/1.4739923.
[37] Butterworth JA, Pao LY, Abramovitch DY. Analysis and comparison of three discrete-time feedforward model-inverse control techniques for nonminimum-phase systems. Mechatronics 2012;22(5):577–87. http://dx.doi.org/10.1016/j.mechatronics.2011.12.006.
[38] Kenton BJ, Leang KK. Design and control of a three-axis serial-kinematic high-bandwidth nanopositioner. IEEE/ASME Trans Mech 2012;17(2):356–69. http://dx.doi.org/10.1109/TMECH.2011.2105499.
[39] Shan Y, Leang KK. Accounting for hysteresis in repetitive control design: nanopositioning example. Automatica 2012;48:1751–8.
[40] Li Y, Bechhoefer J. Feedforward control of a piezoelectric flexure stage for AFM. In: Proc American control conference, Seattle, WA; 2008. p. 2703–9.
[41] Kim K, Zou Q. Model-less inversion-based iterative control for output tracking: piezo actuator example. In: Proc American control conference, Seattle, WA; 2008. p. 2710–5.
[42] Hung S-K. Spiral scanning method for atomic force microscopy. In: Proc tip based nanofabrication workshop, Taipei, Taiwan; 2008. p. 10(1–10).
[43] Mahmood IA, Moheimani SOR, Bhikkaji B. A new scanning method for fast atomic force microscopy. IEEE Trans Nanotechnol 2011;10(2):203–16.
[44] Fleming AJ, Kenton BJ, Leang KK. Bridging the gap between conventional and video-speed scanning probe microscopes. Ultramicroscopy 2010;110(9):1205–14. http://dx.doi.org/10.1016/j.ultramic.2010.04.016.
[45] Tuma T, Lygeros J, Kartik V, Sebastian A, Pantazi A. High-speed multiresolution scanning probe microscopy based on lissajous scan trajectories. Nanotechnology 2012;23:185501.
[46] Bazaei A, Yong YK, Moheimani SOR. High-speed lissajous-scan atomic force microscopy: scan pattern planning and control design issues. Rev Sci Instrum 2012;83(6):063701. http://dx.doi.org/10.1063/1.4725525. <http://link.aip.org/link/?RSI/83/063701/1>.
[47] Yong YK, Fleming AJ, Moheimani SOR. A novel piezoelectric strain sensor for simultaneous damping and tracking control of a high-speed nanopositioner. IEEE/ASME Trans Mech 2013;18(3):1113–21. http://dx.doi.org/10.1109/TMECH.2012.2193895.
[48] Sahoo DR, Sebastian A, Häberle W, Pozidis H, Eleftheriou E. Scanning probe microscopy based on magnetoresistive sensing. Nanotechnology 2011;22(14):145501.
[49] Kartik V, Sebastian A, Tuma T, Pantazi A, Pozidis H, Sahoo DR. High-bandwidth nanopositioner with magnetoresistance based position sensing. Mechatronics 2012;22(3):295–301.
[50] Fleming AJ, Wills AG, Moheimani SOR. Sensor fusion for improved control of piezoelectric tube scanners. IEEE Trans Contr Syst Technol 2008;15(6):1265–6536. http://dx.doi.org/10.1016/j.mechatronics.2007.07.006.
[51] Sebastian A, Pantazi A. Nanopositioning with multiple sensors: a case study in data storage. IEEE Trans Contr Syst Technol 2012;20(2):382–94. http://dx.doi.org/10.1109/TCST.2011.2177982.

Please cite this article in press as: Fleming AJ. Measuring and predicting resolution in nanopositioning systems. Mechatronics (2013), http://dx.doi.org/10.1016/j.mechatronics.2013.10.003